Int. J. Solids Structures Vol. 29, No. 10, pp. 1303–1328, 1992
Printed in Great Britain.

0020–7683/92 $5.00+.00

MICROMECHANICS MODELLING OF ANISOTROPIC DAMAGE IN CROSS-PLY LAMINATES

W. YANG
Department of Engineering Mechanics, Tsinghua University, Beijing 100084, China

and

J. P. BOEHLER
Institut de Mécanique de Grenoble, University Joseph Fourier, Grenoble I,
38041 Grenoble Cedex, France

(*Received* 6 *July* 1990; *in revised form* 5 *September* 1991)

Abstract—A micromechanics model is developed to detail various aspects of anisotropic damage behaviour of cross-ply composite laminates. Attention is focused on multi-ply laminates so that a calculation model can be devised, which is composed of a cracked transversely isotropic ply sandwiched between two self-consistent orthotropic plates of relatively large thickness. Under in-plane loadings restricted to the laminate plane, intralaminar cracks first develop from two families of plies independently, subject to mode I and mode III crack driving forces. The stabilized crack configuration is that of parallel trans-ply cracks with a mutual shielding effect. As the intralaminar cracks touch the interlaminar boundaries, the initial delamination is triggered by large interfacial shear stress and then terminated by a dramatic drop in the driving force. An interaction calculation shows that intralaminar cracking is priviliged at relatively low load level, but then overrun by interlaminar cracking at a relatively high load level. This switch in crack formation constitutes the so-called Characteristic Damage State. By introducing a higher order model allowing shear deformation in the central broken ply, a finite value of the interlaminar shear stress at bonding edges can be achieved. A pseudo-elastic damage behaviour can be predicted, along with the absence of permanent damage strain, if perfect interlaminar adhesion is maintained. The solution in an idealized non-interactive interlaminar slip model is henceforth constructed, which gives rise to permanent damage strain, stabilized hysteresis loop and residual interlaminar stress after unloading.

1. INTRODUCTION

The damage in composite laminates is highlighted by a very organized geometric pattern, especially for cross-plies. This distinctive feature promotes deterministic micromechanics models to demonstrate the gradual damage processes characterized by cracking and localized slip. Recently, many research efforts have been devoted to the micromechanics modelling of composite materials. Budiansky *et al.* (1986) delineated the cracking process of composites reinforced by unidirectional fibres, whereas the overall moduli of such composite plies have been carefully estimated by Dvorak *et al.* (1985), Dvorak and Laws (1987), Laws and Brockenbrough (1987) and Laws and Dvorak (1987), by means of linear elastic fracture mechanics calculations, incorporating self-consistent schemes. For composite laminates, Hashin (1985, 1986, 1987), and Han and Hahn (1988) studied the intralaminar cracking of a sandwich cross-ply by employing either a statically equilibrium or a kinematically admissible field. In contrast to the phenomenological study based on continuum damage theory, e.g. Talreja (1985a, b), the micromechanics study provides more details to the cracking process in composite laminates, and relies on fewer empirical damage characterization parameters.

It is well recognized, for example, from the experimental works of Highsmith and Reifsnider (1982, 1986), and Jamison *et al.* (1984) that the damage development in composite laminates is featured in several stages, namely the initial stabilized intralaminar cracking, the incipiency of interlaminar cracking, the characteristic damage state followed by significant delamination and then concluded by fibre breaking in the favourably oriented plies to final rupture. The experimental data also suggest the existence of a gradually increased permanent damage strain, as well as the localized residual stress. In the present paper, a micromechanics model encompassing the aforementioned features is attempted, with the emphasis on the interaction between intralaminar and interlaminar cracks.

However, the fibre breaking phenomenon in the plies aligned with the load, as well as the gradual rupture of favourably oriented plies are beyond the scope of the present treatment.

2. MICROMECHANICS MODEL

The laminates under consideration are composed of many elastic cross-plies, with particular reference to graphite/epoxy cross-ply laminates assemblied by 16–20 relatively thin plies. The plies belonging to two ply families (1) and (2) orthogonal to each other are alternatively bonded together and subject to the loads lying on the laminate plane, as delineated in Fig. 1. The ply thicknesses of each family are designated by t_1 and t_2, respectively. Obviously, N_{2j} vanish, with x_2 reserved for the thickness direction. Latin indices have a range from 1 to 3 unless notified otherwise, and summation over this range is implied for repeated indices. The average stresses (symbolized by a super-imposed bar) are

$$\bar{\sigma}_{ij} = N_{ij}/t, \tag{1}$$

where t is the total thickness of the laminate. The loading processes can be controlled by the total amount of either displacements or resultant forces; they are related by

$$\bar{\varepsilon}_{ij} = \bar{M}_{ijkl}\bar{\sigma}_{kl}, \tag{2}$$

where $\bar{M}_{ijkl}$ are the macroscopic secant compliance moduli. The conventional matrix notation is adopted

$$\bar{\varepsilon}_\alpha = \bar{M}_{\alpha\beta}\bar{\sigma}_\beta \quad (\alpha, \beta = 1, \ldots, 6), \tag{3}$$

where $\bar{\varepsilon}_\alpha$ and $\bar{\sigma}_\beta$ are sequenced in the standard anticlockwise manner. For example, $\bar{\varepsilon}_1 = \bar{\varepsilon}_{11}, \ldots, \bar{\varepsilon}_6 = 2\bar{\varepsilon}_{12}$, etc.

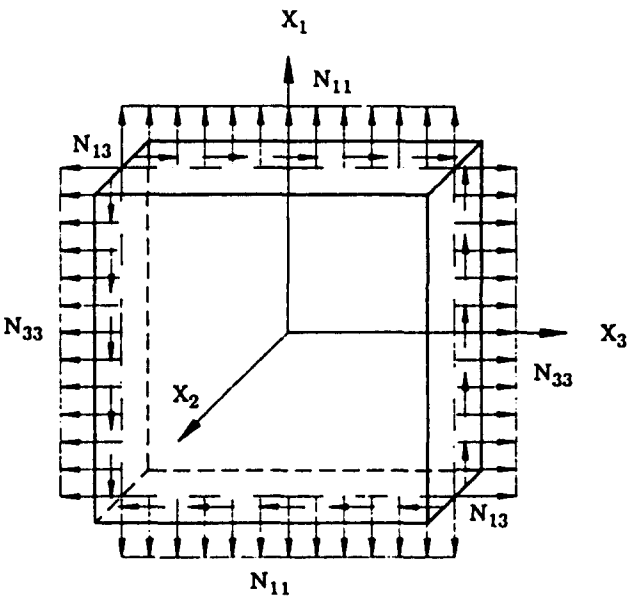

Fig. 1. A rectangular laminate with many cross plies subject to in-plane loading.

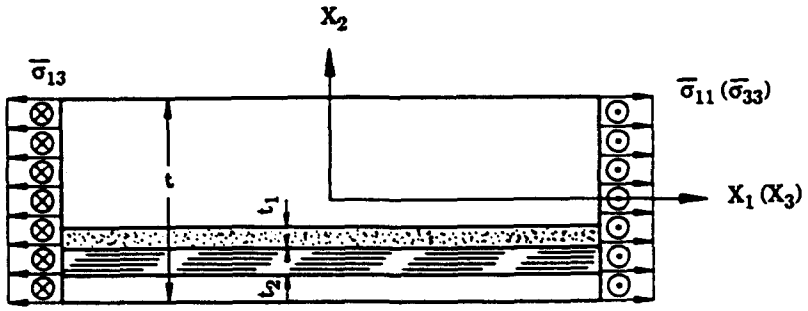

Fig. 2. Reduction to two similar plane problems by the non-interacting assumption for the damage in the two families of plies.

The problem illustrated in Fig. 1 can be decomposed into two almost identical two-dimensional problems as elucidated in Fig. 2, except for the coupling effect produced by the in-plane shear stress $\bar{\sigma}_{13}$. Each problem is further simplified by the presence of only mode I and mode III fractures. Without loss of generality, we only pursue the analysis of the problem residing in the (x_1, x_2) plane. To make it tractable, the multi-ply geometry is approximated by the configuration shown in Fig. 3, that is, a central ply with specific cracking pattern sandwiched by two neighbouring blocks of ply assembly with equivalent damage moduli $\bar{M}_{\alpha\beta}$. Accordingly, the periodic fluctuations in the compliance moduli in the two neighbouring blocks are ignored. As long as the macroscopic compliances for the

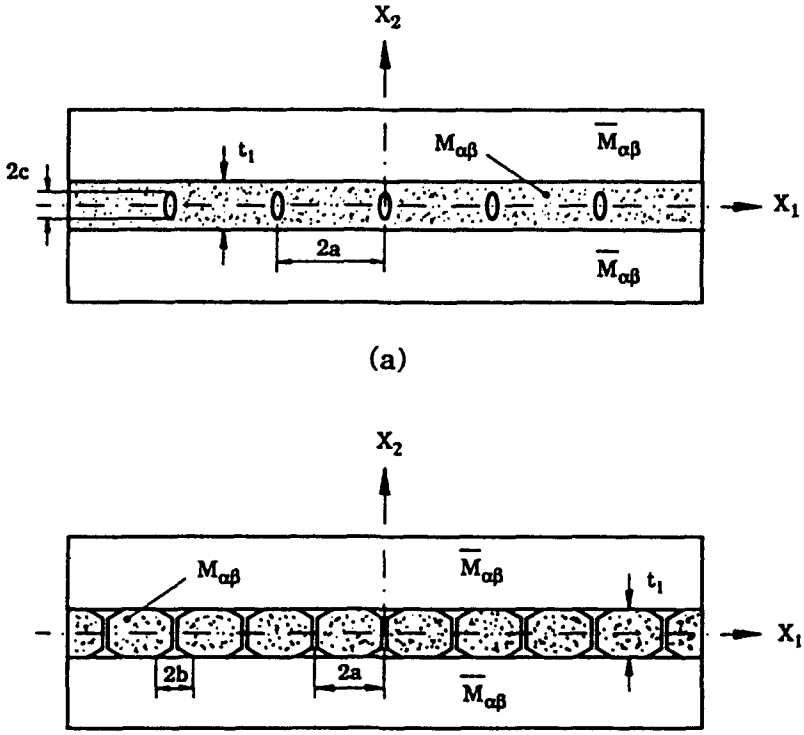

Fig. 3. Sandwich assumption. (a) Initial intralaminar cracking. (b) Interaction between intralaminar and interlaminar cracks.

central ply $M_{\alpha\beta}^{(1)}$ (as well as $M_{\alpha\beta}^{(2)}$ in the similar problem) are obtained, $\bar{M}_{\alpha\beta}$ can be evaluated by a simple mixture rule:

$$\bar{M}_{\alpha\beta}^{-1} = c_1 M_{\alpha\beta}^{(1)-1} + c_2 M_{\alpha\beta}^{(2)-1}, \tag{4}$$

where c_1 and c_2 are the thickness fractions of plies belonging to families (1) and (2), respectively. The damaged moduli for the single ply ($M_{\alpha\beta}^{(1)}$ or $M_{\alpha\beta}^{(2)}$) can be calculated from

$$M_{\alpha\beta}^{(1)} = M_{\alpha\beta} + D_{\alpha\beta}^{(1)}, \text{ etc.} \tag{5}$$

where $D_{\alpha\beta}^{(1)}$ are the damage-induced compliances and can be calculated from the macroscopic damage strains:

$$\bar{\varepsilon}_\alpha^{D(1)} = D_{\alpha\beta}^{(1)} \bar{\sigma}_\beta^{(1)}, \text{ etc.} \tag{6}$$

The uncracked moduli, $M_{\alpha\beta}$, are measurable from a single-ply specimen, and should have the symmetry of transverse isotropy described by:

$$M_{\alpha\beta} = \begin{bmatrix} \frac{1}{E} & -\frac{\nu}{E} & -\frac{\nu_z}{E} & 0 & 0 & 0 \\ -\frac{\nu}{E} & \frac{1}{E} & -\frac{\nu_z}{E} & 0 & 0 & 0 \\ -\frac{\nu_z}{E} & -\frac{\nu_z}{E} & \frac{1}{E_z} & 0 & 0 & 0 \\ 0 & 0 & 0 & \frac{1}{G_z} & 0 & 0 \\ 0 & 0 & 0 & 0 & \frac{1}{G_z} & 0 \\ 0 & 0 & 0 & 0 & 0 & \frac{2(1+\nu)}{E} \end{bmatrix}_{(\ldots z)}, \tag{7}$$

where z labels the fibre direction as well as the axis of transverse isotropy. For plies belonging to family (1) and family (2) z corresponds to x_3 and x_1 axes, respectively. The macroscopic moduli for cracked plies, $M_{\alpha\beta}^{(1)}$ and $M_{\alpha\beta}^{(2)}$, as well as their average $\bar{M}_{\alpha\beta}$ through (4), are orthotropic.

3. FORMATION OF INITIAL INTRALAMINAR CRACKS

At the initial stage of intralaminar crack formation, the interlaminar shear stress transmitted through the bonding seems to be negligible under remote uniform displacement loading. A non-interacting calculation is then conducted on the central ply, weakened by a stack of parallel intralaminar cracks, as described in Fig. 4. Extended by periodicity, the

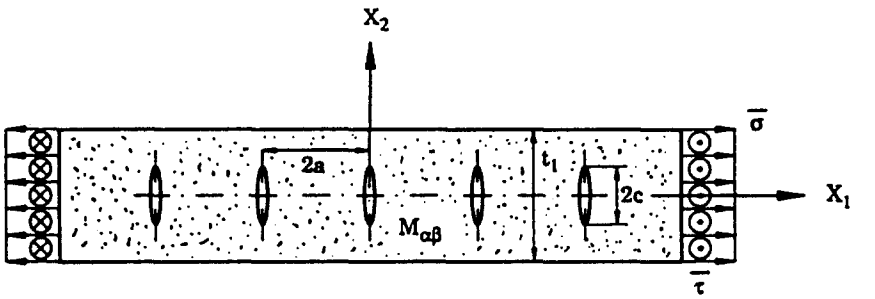

Fig. 4. A central ply weakened by a stack of parallel cracks with interlaminar interaction neglected.

problem in Fig. 4 is similar to the problem of double periodic crack arrays in an infinite transversely isotropic medium. Its solution can be approached through the continuous dislocation distribution method by Bilby and Eshelby (1968). The solution is simplified by the recognition that those straight dislocations are aligned with the transverse isotropy axis. Without entering the details of the formulation [the procedure for the mode I in the isotropic case is illustrated by Delameter *et al.* (1975)], it can be shown that the dislocation distribution functions D_I and D_{III} for mode I and mode III fractures are governed by the following uncoupled singular integral equations:

$$\int_{-c}^{c} D_{I,III}(x_2')\left[\frac{1}{x_2'-x_2}+\Gamma_{I,III}(x_2,x_2')\right]dx_2' = \varepsilon_{I,III}, \tag{8}$$

for all x_2 belonging to the range $(-c, c)$, argumented with the closing condition of cracks:

$$\int_{-c}^{c} D_{I,III}(x_2)\,dx_2 = 0. \tag{9}$$

The regular kernels Γ_I and Γ_{III} for mode I and mode III cracking are:

$$\Gamma_I(x_2,x_2') = \frac{1}{x_2-x_2'}+\sum_{n=-\infty}^{\infty}\left\{\frac{\pi}{a}\coth\left[\frac{\pi}{2a}(x_2'-x_2+nt_1)\right]\right.$$
$$\left.-\left(\frac{\pi}{2a}\right)^2(x_2'-x_2+nt_1)\sinh^{-2}\left[\frac{\pi}{2a}(x_2'-x_2+nt_1)\right]\right\},$$
$$\Gamma_{III}(x_2,x_2') = \frac{1}{x_2-x_2'}+\frac{\pi}{2a}\sum_{n=-\infty}^{\infty}\coth\left[\frac{\pi}{2a}(x_2'-x_2+nt_1)\right], \tag{10}$$

where the geometric parameters a, c and t_1 are elucidated in Figs 3 and 4. The applied strains ε_I and ε_{III} for the dislocation formation are:

$$\varepsilon_I = 4\pi(1-\nu_z^2)\frac{\bar{\sigma}}{E}, \quad \varepsilon_{III} = 2\pi\frac{\bar{\tau}}{G_z}, \tag{11}$$

where the notation of the material constant in (7) is preserved.

It is recognized in the literature that singular integral equations like (8) produce solutions possessing square root singularity at both ends. Therefore, if one writes:

$$D_{I,III}(x_2) = \frac{B_{I,III}(u)}{\pi\sqrt{1-u^2}}, \quad u = \frac{x_2}{c}, \tag{12}$$

then B_I and B_{III} are skew-symmetric, dimensionless functions bounded uniformly in the closed interval $[-1, 1]$. Their solutions can be effectively obtained by the Gaussian–Chebyshev integration formula developed by Erdogan (1980). The results rely on two dimensionless parameters p and q defined by:

$$p = \frac{a}{c}, \quad q = \frac{t_1}{2c}. \tag{13}$$

It can be established that the stress intensity factors K_I and K_{III} relate to the end values of B_I and B_{III} by:

$$K_{\mathrm{I}} = \bar{\sigma}\sqrt{\pi c}B_{\mathrm{I}}(1), \quad K_{\mathrm{III}} = \bar{\tau}\sqrt{\pi c}B_{\mathrm{III}}(1). \tag{14}$$

The non-dimensionalizations in (12) are engaged in such a way that $B_{\mathrm{I}}(1)$ and $B_{\mathrm{III}}(1)$ are exactly the ratios between the stress intensity factors of double period cracks and those of a single crack in an infinite medium, as justified in (14). $B_{\mathrm{I}}(1)$ and $B_{\mathrm{III}}(1)$ are plotted versus p for a set of q values in Fig. 5, and their values for an array of p and q settings are listed in Tables 1 and 2. The results presented in Table 1 are virtually identical to those from the same problem, calculated by Delameter *et al.* (1975) from a somewhat lengthy computational scheme. For both mode I and III cases, the calculations indicate an unstable tendency for cracks growing toward the interlaminar boundary, as well as a stable shielding effect by the birth of parallel cracks. This suggests that the intralaminar cracks will propagate rapidly towards the interlaminar boundary. Blocked by a favourably oriented ply, the further crack propagation will be predominantly in the x_3 direction, as illustrated by Dvorak and Laws (1987). For initial intralaminar cracking, the crack opening displacements δ_{I} and δ_{III} are given by:

$$\delta_{\mathrm{I,III}}(x_2) = \frac{c\varepsilon_{\mathrm{I,III}}}{\pi}\int_{-1}^{u}\frac{B_{\mathrm{I,III}}(s)}{\sqrt{1-s^2}}\,\mathrm{d}s \equiv c\varepsilon_{\mathrm{I,III}}\Delta_{\mathrm{I,III}}(u), \tag{15}$$

following from (12) and the kinematics of crack dislocation. By the property of the Chebyshev polynomials, $\Delta_{\mathrm{I,III}}$ in (15) can be directly summed as:

$$\Delta_{\mathrm{I,III}}(u_j) = \frac{1}{2m}\sum_{k=j+1}^{2m} B_{\mathrm{I,III}}(s_k); \quad j = 1,\ldots,2m-1, \tag{16}$$

where

$$u_j = \cos\left(\frac{j\pi}{2m}\right), \quad s_k = \cos\left(\frac{2k-1}{4m}\pi\right), \quad j,k = 1,\ldots,m, \tag{17}$$

are the zeros of the Chebyshev polynomials $T_{2m}(s_k)$ and $U_{2m-1}(u_j)$, respectively. The macropscopic damage strain $\bar{\varepsilon}_{ij}^{\mathrm{D}}$ caused by the crack opening is

$$\bar{\varepsilon}_{11,13}^{\mathrm{D}} = \frac{1}{2at_1}\int_{-c}^{c}\delta_{\mathrm{I,III}}(x_2)\,\mathrm{d}x_2. \tag{18}$$

Substituting (15) and exchanging the order of integration, one arrives at:

$$\bar{\varepsilon}_{11,13}^{\mathrm{D}} = \varepsilon_{\mathrm{I,III}}g_{\mathrm{I,III}}(p,q), \tag{19}$$

where

$$g_{\mathrm{I,III}}(p,q) = \frac{\pi}{pq(4m+1)}\sum_{k=1}^{m} s_k B_{\mathrm{I,III}}(s_k). \tag{20}$$

Functions $g_{\mathrm{I,III}}$ depend only on the geometric parameters p and q and solely characterize the effect of crack geometry on the macroscopic damage strains, henceforth the overall moduli; g_{I} and g_{III} are tabulated in Tables 3 and 4 for the same array of the (p,q) parameters.

The combination of (5) and (19) furnishes the secant moduli for the cracked central ply of family (1):

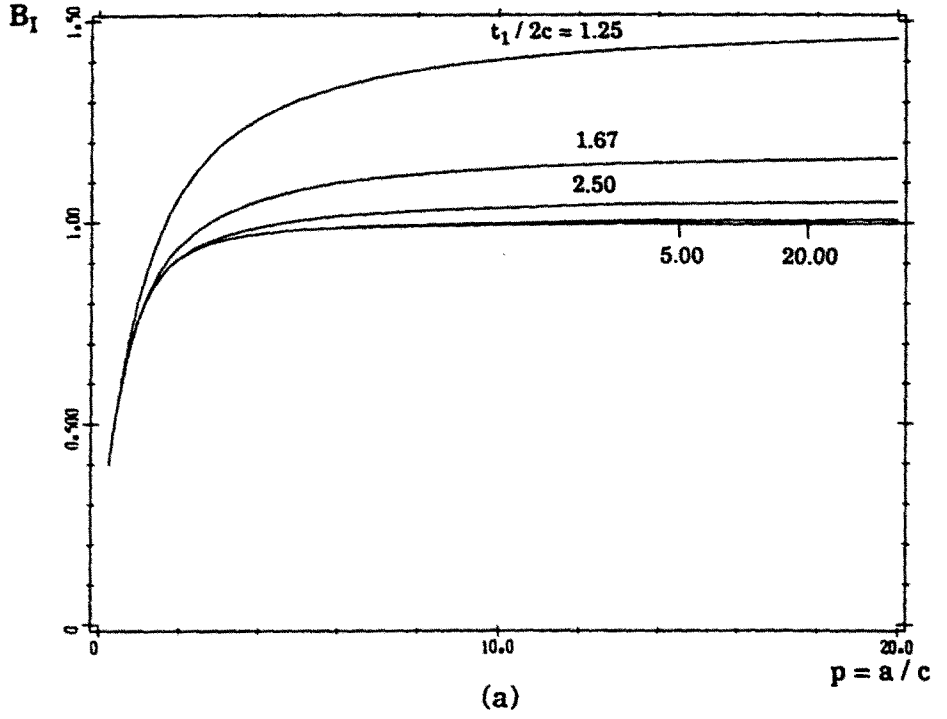

(a)

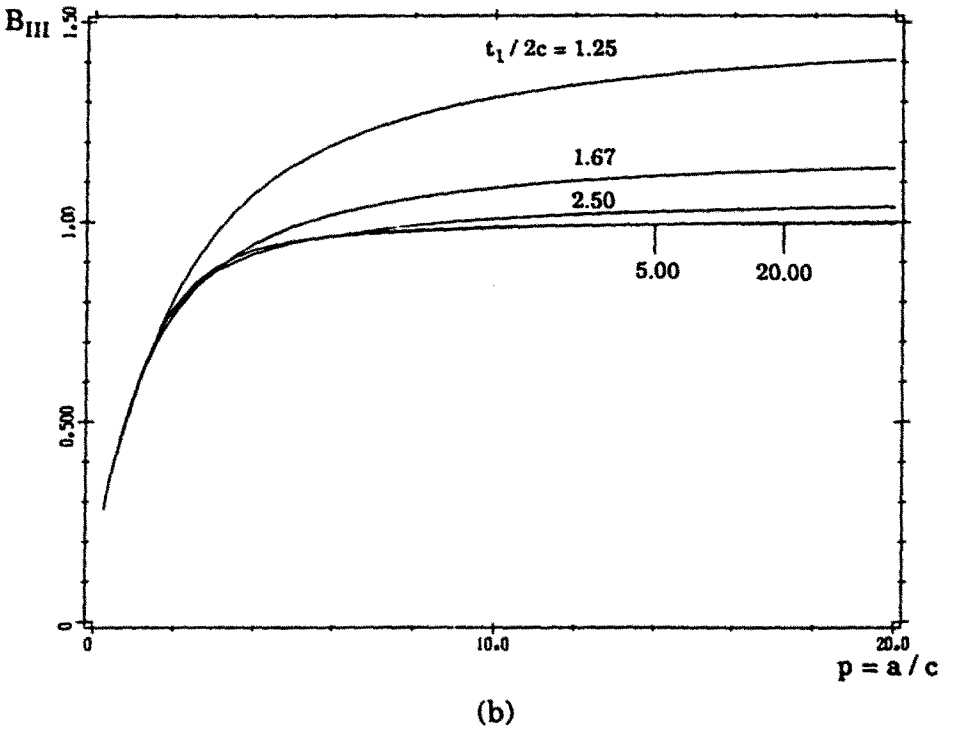

(b)

Fig. 5. Dimensionless stress intensity factors for the initial intralaminar cracking. (a) Mode I. (b) Mode III.

$$M_{11}^{(1)} = \frac{1}{E}[1+4\pi(1-\nu_z^2)g_1(p,q)], \quad M_{33}^{(1)} = \frac{1}{G_z}[1+2\pi g_{III}(p,q)]. \tag{21}$$

An identical procedure can be employed for the plies of family (2). After using the mixture rule (4), we finally arrive at:

Table 1. Dimensionless stress intensity factor of intralaminar cracking, mode I

a/c	$t_1/2c = 20.00$	5.00	2.50	1.67	1.25
20.00	0.99678	1.00134	1.03912	1.13674	1.4066
10.00	0.98794	0.98575	1.00871	1.08589	1.31057
5.00	0.95412	0.95175	0.94833	0.98927	1.14369
4.00	0.93095	0.92980	0.92025	0.94535	1.07210
3.00	0.88638	0.88614	0.87523	0.87966	0.96889
2.00	0.78960	0.78960	0.78487	0.77188	0.81100
1.00	0.57028	0.57028	0.57020	0.56507	0.55730
0.50	0.39895	0.39895	0.39895	0.39881	0.39209
0.25	0.28210	0.28210	0.28210	0.28210	0.28210

Table 2. Dimensionless stress intensity factor of intralaminar cracking, mode III

a/c	$t_1/2c = 20.00$	5.00	2.50	1.67	1.25
20.00	0.99904	1.00850	1.05318	1.16089	1.45599
10.00	0.99597	1.00098	1.03836	1.13527	1.40456
5.00	0.98412	0.98495	1.00716	1.08324	1.30672
4.00	0.97554	0.97583	0.99162	1.05768	1.26085
3.00	0.95798	0.95802	0.96626	1.01678	1.18953
2.00	0.91380	0.91380	0.91569	0.94240	1.06578
1.00	0.76417	0.76417	0.76419	0.76709	0.81075
0.50	0.56316	0.56316	0.56316	0.56320	0.56944
0.25	0.39896	0.39896	0.39896	0.39896	0.39896

Table 3. Normalized damage strain for intralaminar cracking, mode I

a/c	$t_1/2c = 20.00$	5.00	2.50	1.67	1.25
20.00	0.00097	0.00391	0.00811	0.01325	0.02112
10.00	0.00193	0.00770	0.01573	0.02521	0.03909
5.00	0.00373	0.01487	0.02958	0.04582	0.06778
4.00	0.00454	0.01815	0.0589	0.05475	0.07936
3.00	0.00576	0.02302	0.04548	0.06798	0.09563
2.00	0.00762	0.03050	0.06069	0.08928	0.12019
1.00	0.01017	0.04068	0.08135	0.12146	0.15902
0.50	0.01134	0.04535	0.09069	0.13603	0.18057
0.25	0.01189	0.04755	0.09510	0.14264	0.19019

Table 4. Normalized damage strain for intralaminar cracking, mode III

a/c	$t_1/2c = 20.00$	5.00	2.50	1.67	1.25
20.00	0.00098	0.00394	0.00824	0.01358	0.02198
10.00	0.00195	0.00782	0.01622	0.02648	0.04222
5.00	0.00384	0.01539	0.03144	0.05038	1.07810
4.00	0.00476	0.01906	0.03969	0.06144	0.09403
3.00	0.00623	0.02494	0.05026	0.07870	0.11805
2.00	0.00890	0.03561	0.07134	0.10934	0.15840
1.00	0.01457	0.05827	0.11655	0.17513	0.23920
0.50	0.01940	0.07761	0.15522	0.23283	0.31112
0.25	0.02213	0.08853	0.17705	0.26558	0.35410

$$\bar{M}^{-1}_{11,33} = c_{2,1}E_z + c_{1,2}\frac{E}{1+4\pi(1-\nu_z^2)g_1(p,q)}, \quad \bar{M}_{55} = M^{(1)}_{55} = M^{(2)}_{55}, \tag{22}$$

whereas the other compliance moduli are unaffected by the cracking. A simplified scheme for the micromechanics calculation on double period cracks was carried out by Aboudi (1987) under an approximate cell model. Under the special case of homogeneous and isotropic materials, his approximate estimate agreed fairly well with the exact solution of Delameter *et al.* (1975) [which is identical to the present analysis under the said situation, as shown in Figs 2 and 4 of Aboudi's work (1987)]. The above results will become transparent if we can cast them in terms of the average longitudinal and transverse moduli $\bar{E}_z$ and $\bar{E}$ normalized by the respective non-damaged counterparts $\bar{E}_{z0}$ and $\bar{E}_0$.

$$\frac{\bar{E}_z}{\bar{E}_{z0}} = \frac{\bar{E}}{\bar{E}_0} = 1 - \frac{1-c_a}{(1+\beta c_a)} \cdot \frac{1}{1+\alpha/g_1(p,q)}, \tag{23}$$

where

$$\alpha = [4\pi(1-\nu_z^2)]^{-1}, \quad \beta = \frac{E_z}{E} - 1, \tag{24}$$

and c_a is the thickness fraction of the plies aligned in the sense of the corresponding tensile moduli. The value of α defined in (24) is about 0.1. Accordingly, the case of $g_1(p,q)$ much less than 0.1 would roughly predict an undamaged modulus, whereas the case of $g_1(p,q)$ substantially larger than 0.1 would indicate a modulus correlating to the ply-discount prediction. As one can find from Table 3, $g_1(p,q)$ can be very small for sparsely distributed cracks and reach 0.2 for reasonably dense cracks. It is also shown clearly from (23) that the increase in c_a (the thickness fraction of the aligned plies) would effectively prevent the stiffness reduction. All the above results agree qualitatively with the stiffness measurements of Allen *et al.* (1987) and Groves *et al.* (1987) for Hercules AS4/3502 laminates, where the two parameters α and β in (24) are taken as 0.088 and 14.1 respectively. Their testing stiffness data, as shown in the solid curves of Fig. 6, concern intralaminar cracks occupying the whole thickness of the plies. The constraining effect due to aligned neighbouring plies, however, motivates our tentative taking of $q = 1.15$ in our periodic configuration referring to Fig. 4. The value of p can be determined by the number of cracks per inch measured in their paper, together with the ply-thickness of 0.005 in. which they later specified in their finite element model. The resulting theoretical predictions according to (23), as shown in the dashed curves of Fig. 6, agree very well with the experiment data by Groves *et al.* (1987) and Allen *et al.* (1987) for all cases. The same qualitative agreement with the experimental data by Ogin *et al.* (1985) for GFRP laminates, is also observed. We emphasize that the

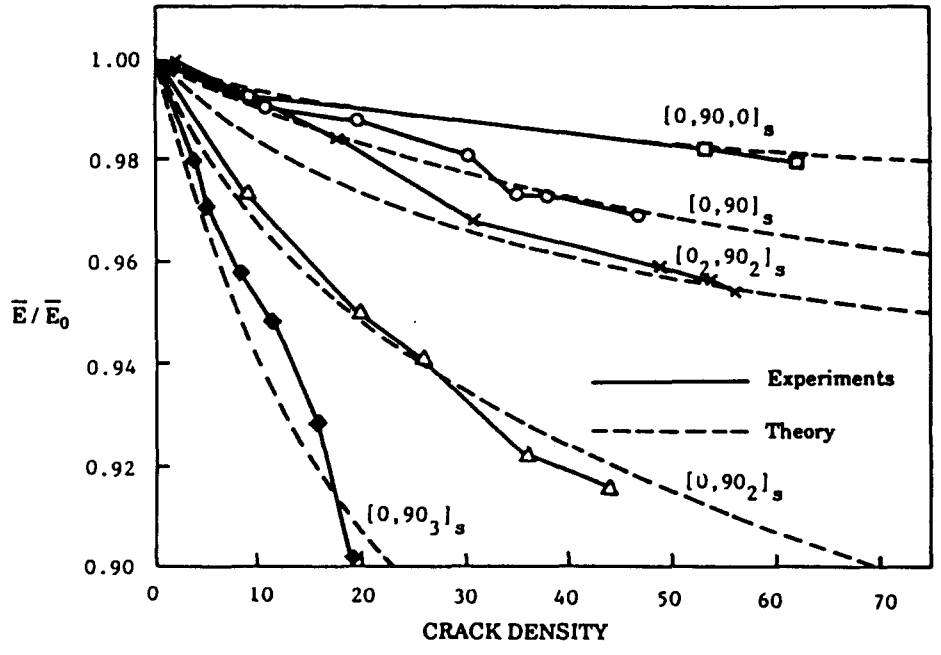

Fig. 6. The stiffness reduction by intralaminar cracking of several cross-ply laminates, vs the crack density (number of cracks per inch of the ply thickness). Solid curves marked by symbols: the experimental data by Groves *et al.* (1987); dashed curves: theoretical predictions from (23), $q = 1.15$.

present prediction (23) does not contain adjustable constants like most continuum damage theories.

The changes in the Poisson's ratios can be worked out from (22) and (7) as

$$\frac{\bar{\nu}}{\bar{\nu}_0} = \frac{\bar{\nu}_z}{\bar{\nu}_{z0}} = \frac{\bar{E}}{\bar{E}_0}, \tag{25}$$

where $\bar{\nu}_0$ and $\bar{\nu}_{z0}$ are the undamaged values of $\bar{\nu}$ and $\bar{\nu}_z$ with $\bar{E}/\bar{E}_0$ given in (23). The decline in the average Poisson's ratios with the progression of microcracking agrees with the test data.

4. INTRALAMINAR–INTERLAMINAR INTERACTION

We next turn to a discussion on the co-existence of intralaminar and interlaminar cracks, as depicted in Fig. 3(b). For many ply laminates, the outside free surfaces seem to have negligible effect on the central broken ply; then Fig. 3(b) reduces to the situation in Fig. 7 by symmetry. According to Erdogan and Civelek (1974), such a simplification is justified if the ply number exceeds 10. The intralaminar cracks have a spacing $2a$ and the interlaminar cracks have a one-side length b less than a. The decomposition into a plane strain problem and an anti-plane shear problem is again observed. The periodicity on the central ply cracking pattern is assumed for mathematical tractability. Attention will be directed mostly to the plane strain problem; parallel results for the anti-plane shear problem will also be listed at appropriate places.

As a first step, we detach the bonding interface and replace it with a periodic shear interaction stress $\tau_1(x_1)$. The normal interaction stress is omitted because it is predominantly compressive and altogether insignificant for a thin ply situation. The lower half-plane in Fig. 7 is composed of an equivalent orthotropic medium with secant compliances $\bar{M}_{ij}$. Under remote stress $\bar{\sigma}$, a uniform strain differential

$$\bar{\varepsilon} = \left(\bar{M}_{11} - \frac{\bar{M}_{13}^2}{\bar{M}_{33}}\right)\bar{\sigma} \equiv \bar{\sigma}/\bar{E}, \tag{26}$$

occurs under plane strain constraints. Additionally, the interfacial shear stress $\tau_1(x_1)$ produces an interfacial tensile strain:

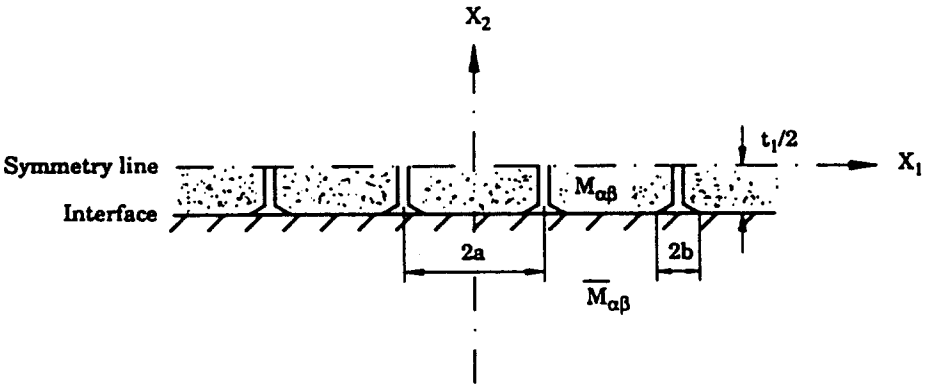

Fig. 7. A broken ply symmetrically sandwiched between infinite blocks.

$$\varepsilon(x_1) = \frac{-\hat{S}}{\bar{E}a}\int_{b-a}^{a-b} \cot\left[\frac{\pi(x_1'-x_1)}{2a}\right]\tau_1(x_1')\,dx_1'. \tag{27}$$

This result can be established by the complex variable theory for anisotropic plane elasticity. The dimensionless constant $\hat{S}$ in (27) only involves the material moduli $\bar{M}_{\alpha\beta}$. Specifically,

$$\hat{S} = \mathrm{Im}\left\{\frac{s_1+s_2}{2}\right\}, \tag{28}$$

where s_1 and s_2 are the roots of the characteristic equation of the particular solid:

$$s_{1,2} = \sqrt{-\frac{\bar{b}_{12}+\frac{1}{2}\bar{b}_{66}\pm\bar{D}}{\bar{b}_{11}}}, \quad \bar{D} = \sqrt{(\bar{b}_{12}+\tfrac{1}{2}\bar{b}_{66})^2-\bar{b}_{11}\bar{b}_{22}}. \tag{29}$$

s_1 and s_2 also serve as the coefficients of x_2 in composing two analytical functions of $z_\alpha = x_1+s_\alpha x_2$, $\alpha = 1, 2$. If $\bar{D}$ is real (which is usually the case for graphite/epoxy composite laminates), s_1 and s_2 are purely imaginary. $\bar{D}$ vanishes for transversely isotropic materials. The quantities $\bar{b}_{11}$, $\bar{b}_{12}$, $\bar{b}_{22}$ and $\bar{b}_{66}$ in (29) are the plane strain macroscopic compliance moduli. They are given by:

$$\bar{b}_{11} = \bar{E}^{-1}, \quad \bar{b}_{12} = \bar{M}_{12}-\frac{\bar{M}_{13}\bar{M}_{23}}{\bar{M}_{33}}, \quad \bar{b}_{22} = \bar{M}_{22}-\frac{\bar{M}_{23}^2}{\bar{M}_{33}}, \quad \bar{b}_{66} = \bar{M}_{66}. \tag{30}$$

The broken thin ply is treated by a higher order plate theory subject to plane strain constraints. Specifically, the displacement field in the broken thin ply is approximated by:

$$u_1^{(1)} = w_0(x_1)+w_2(x_1)\left(\frac{2x_2}{t_1}\right)^2, \quad u_2^{(1)} = \bar{\varepsilon}_y x_2, \quad u_3^{(1)} = 0. \tag{31}$$

Here, the symmetry condition with respect to x_2 has already been enforced. If w_2 is set to zero, as frequently assumed in the literatures for similar problems, (31) reduces to the plane stress theory of thin ply. However, the incorporation of w_2 permits a shear deformation mode, which is compatible with interfacial shear loading and provides some interesting insights to the problem; (31) is similar to the deformation mode assumed by Han and Hahn (1988) applied to sandwich composite cross-plies.

Under assumption (31), the kinematic conditions and all the continuity requirements can be pointwisely satisfied, but the equilibrium equation can only be obeyed in a thickness average sense. Using the transverse isotropy moduli as noted in (7), the interfacial tensile strain of the broken plies is:

$$\varepsilon^{(1)}(x_1) = \frac{(1+\nu)t_1}{3E}\tau_1'(x_1) - \frac{2(1+\hat{\nu}^2)}{E(1-\nu\nu_z)t_1}\int_{b-a}^{x_1}\tau_1(x_1')\,dx_1' - \hat{\nu}\bar{\varepsilon}_y, \tag{32}$$

where

$$\hat{\nu} = \frac{\nu(1+\nu_z)}{1-\nu\nu_z}, \tag{33}$$

is a compound Poisson's ratio. In (31), the lateral contraction strain ε_y is approximated by its average $\bar{\varepsilon}_y$; the latter should be consistent with the lateral deformation of the neighbouring equivalent medium

$$\bar{\varepsilon}_y = \bar{b}_{12}\bar{\sigma}. \tag{34}$$

On the other hand, $\bar{\varepsilon}_y$ can be inferred by requiring that the average interfacial normal pressure vanishes:

$$\bar{\varepsilon}_y = -\hat{\nu}\bar{\varepsilon}^{(1)}, \tag{35}$$

where

$$\bar{\varepsilon}^{(1)} = \frac{1}{2(a-b)}\int_{b-a}^{a-b} \varepsilon^{(1)}(x_1)\,\mathrm{d}x_1, \tag{36}$$

is the average interfacial strain of the thin ply. Supposing that the interlaminar bonding can withhold perfect adhesion at this moment, we derive an interfacial strain compatibility equation from (26), (27), (32) and (35):

$$f_\varepsilon(u) - \varepsilon^2 f_\varepsilon''(u) = \frac{\Lambda}{\pi}\int_{-1}^{1} \eta \cot[\eta(s-u)]\,\mathrm{d}f_\varepsilon(s) - 1. \tag{37}$$

Equation (37) is cast in a dimensionless form to suit both plane strain and antiplane shear situations. The derivation for the latter case is omitted here. In (37), we have:

$$u = \frac{x_1}{a-b}, \quad \eta = \frac{\pi}{2}\left(1 - \frac{b}{a}\right), \quad \Lambda = \frac{\lambda t_1}{a-b}, \tag{38}$$

and

$$f_\varepsilon(u) = \frac{2}{E\bar{\varepsilon}t_1}\frac{1+\hat{\nu}^2}{1-\nu\nu_z}\int_{b-a}^{x_1} \tau_1(x_1')\,\mathrm{d}x_1',$$

$$\varepsilon = \sqrt{\frac{2(1+\nu)(1-\nu\nu_z)}{3(1+\hat{\nu}^2)}}\,\frac{t_1}{2(a-b)},$$

$$\bar{\varepsilon} = \frac{\bar{\sigma}}{\bar{E}} - \hat{\nu}^2\bar{\varepsilon}^{(1)}, \quad \lambda = \hat{S}\frac{E}{\bar{E}}\frac{1-\nu\nu_z}{1+\hat{\nu}^2}, \tag{39}$$

for plane strain problems, and

$$f_\varepsilon(u) = \frac{2}{G_z\bar{\varepsilon}t_1}\int_{b-a}^{x_1} \tau_3(x_1')\,\mathrm{d}x_1',$$

$$\varepsilon = \frac{1}{\sqrt{3}}\frac{t_1}{2(a-b)},$$

$$\bar{\varepsilon} = \bar{M}_{55}\bar{\tau}, \quad \lambda = \tfrac{1}{2}G_z\sqrt{\bar{M}_{44}\bar{M}_{55}}, \tag{40}$$

for anti-plane shear problems.

It is observed that ε is a small parameter for well-spaced intralaminar cracks. The asymptotic limit

$$f(u) = \lim_{\varepsilon\to 0} f_\varepsilon(u) \tag{41}$$

is governed by the degenerated eqn (37):

$$\frac{\Lambda}{\pi}\int_{-1}^{1}\eta\cot[\eta(s-u)]\,df(s)-f(u)=1,\quad f(\pm 1)=0. \tag{42}$$

Equation (42) is a singular integro-differential equation with a Hilbert kernel. Equations of this type have been discovered in Prandtl air foil theory [e.g. Vekua (1945)], stiffener stress diffusion (Arutiunian and Mkhitarian, 1969) and thin film deposition (Yang, 1984). The genererate form (42) will arrive directly if a plane stress theory for the broken thin ply is adopted. We intend to concentrate on (42) in the most part in this paper. The behaviour of the solution for the perturbed eqn (37) will be discussed in Section 6.

As established rigorously by Arutiunian and Mkhitarian (1969), the normalized interfacial shear stress

$$\tau(u)=f'(u), \tag{43}$$

has singularities at $u=\pm 1$, and can be represented by:

$$\tau(u)=\frac{T(u)}{\sqrt{\cos(2\eta u)-\cos(2\eta)}}, \tag{44}$$

where $T(\pm 1)$ is bounded and non-zero. From (38) and (44), one concludes that $\tau(u)$ has a square root singularity near the bonding edges as long as $b\neq 0$. As b tends to zero, however, the singularity strengthens to a simply reverse singularity $T(u)/[\sqrt{2}\cos(\pi u/2)]$. This observation indicates an immediate delamination as soon as the intralaminar cracks reach the interlaminar bounding surface. The immediate initial growth of interlaminar cracks underlines the necessity to include the interaction between interlaminar and intralaminar cracks. As this phenomenon is understood, we move on to discuss the case with non-zero b, in which one has:

$$\tau(u)=\frac{B(u)}{\sqrt{1-u^2}},\quad u\in(-1,1), \tag{45}$$

where $B(u)$ is a uniformity bounded, skew-symmetric function. Utilizing the same procedure outlined in Section 3, we obtain the following linear algebraic equations to determine the values of B at positive discrete points $s_k(k=1,\ldots,m)$ corresponding to the zeros of the Chebyshev polynomial T_{2m}:

$$\sum_{k=1}^{m}(\Lambda\eta\{\cot[\eta(s_k-u_j)]+\cot[\eta(s_k+u_j)]\}+\pi H(j-k+\tfrac{1}{2}))B(s_k)=2m,\quad j=1,\ldots,m, \tag{46}$$

where s_k and u_j are given in (14) and $H(\bullet)$ is the Heaviside step function. The interlaminar stress intensity factors K_1 and K_3 can be computed from:

$$K_{1,3}=\lim_{x_1\to a-b}\sqrt{2\pi(a-b-x_1)}\tau_{1,3}(x_1), \tag{47}$$

by their conventional definitions. Combining the above formula with (39), (40), (41), (43) and (45), one arrives at:

$$K_{1,3}=\hat{\sigma}_{1,3}\sqrt{t_1}k, \tag{48}$$

where

$$\hat{\sigma}_1 = \left[\bar{\sigma} - \frac{\hat{\nu}^2}{\bar{E}}\bar{\varepsilon}^{(1)}\right]\sqrt{\frac{E}{2\bar{S}E}\frac{1-\nu\nu_z}{1+\hat{\nu}^2}},$$

$$\hat{\sigma}_3 = \bar{\tau}\left(\frac{\bar{M}_{55}}{\bar{M}_{44}}\right)^{1/4}\sqrt{G_z\bar{M}_{55}}, \tag{49}$$

and

$$k = \sqrt{\frac{\pi\Lambda}{2}}B(1) = k(\eta, \Lambda), \tag{50}$$

is the normalized interlaminar intensity factor. The factorization in (48) separates the three ingredients in the composition of the interlaminar stress intensity factor; $\hat{\sigma}_{1,3}$ represents explicitly the effect of the loading and the material constants, whereas the second term gives the square root dependence of the interlaminar K on the ply thickness. The first two terms are irrelevent to any change of the crack geometries which might occur during the interaction. In contrast, the third term, k, solely represents and depends only on the crack geometric pattern. Through a theoretical analysis involving the Melin transformation, it can be shown, Koiter (1955), that:

$$\lim_{\Lambda \to 0} k(\eta, \Lambda) = 1, \quad \text{for} \quad \eta < \frac{\pi}{2}. \tag{51}$$

The various values of k for different $2a/(\lambda t_1)$ and $2b/(\lambda t_1)$ are documented in Table 5.

5. CHARACTERISTIC DAMAGE STATE

We now look closely at the variation of k with respect to the two parameters a and b representing the intralaminar crack density and the degree of delamination, respectively. As shown in Fig. 8(a), at fixed a values (or at a fixed intralaminar crack geometry), k tends to infinity when b approaches zero, as argued in (44) for the reason of immediate initial delamination. This initial delamination, however, soon arrests, due to the short range nature of the interaction between two neighbouring bonding edges. Therefore, if the delamination is governed by the interlaminar stress intensity factors K_1 and K_3:

$$K_1 = K_{1c}, \quad K_3 = K_{3c}, \tag{52}$$

with critical values K_{1c} and K_{3c} denoting the decohesion resistance of the interlaminar bonding, one concludes that only a small amount of delamination is accumulated at the beginning of the damage, due to the extremely stable character of the initial delamination, as evidenced by the rapidly descending curves in Fig. 8(a) for small b values.

Table 5. Dimensionless interlaminar stress intensity factor

$2b/\lambda t_1$	$2a/\lambda t_1 = 10.00$	12.00	15.00	20.00	30.00
0.125	1.41730	1.41832	1.41822	1.41854	1.41665
0.250	1.26687	1.26824	1.26908	1.26917	1.26785
0.500	1.16188	1.16382	1.16516	1.16569	1.16483
1.000	1.09015	1.09310	1.09529	1.09652	1.09624
2.000	1.04053	1.04550	1.04929	1.05177	1.05241
3.000	1.01697	1.02421	1.02973	1.03346	1.03498
5.000	0.98493	0.99906	1.00903	1.01565	1.01900
7.500	0.92950	0.97041	0.99152	1.00348	1.00953
9.000	0.81416	0.94220	0.98042	0.99770	1.00584
9.500	0.68652	0.92699	0.97607	0.99584	1.00478
9.750	0.54406	0.91726	0.97371	0.99490	1.00427
9.875	0.41118	0.91165	0.97246	0.99443	1.00402

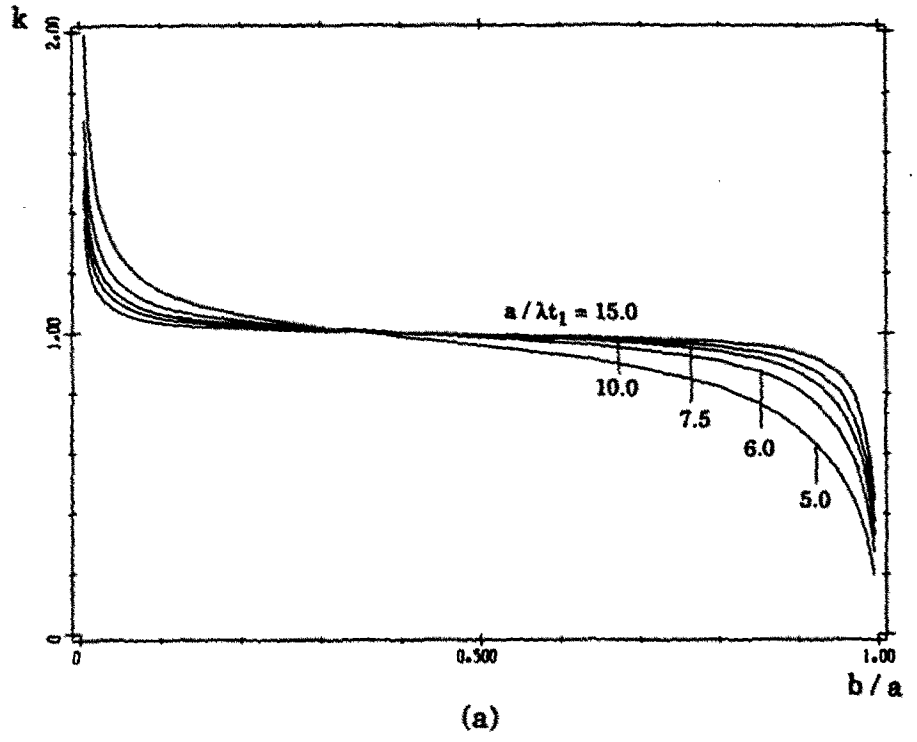

(a)

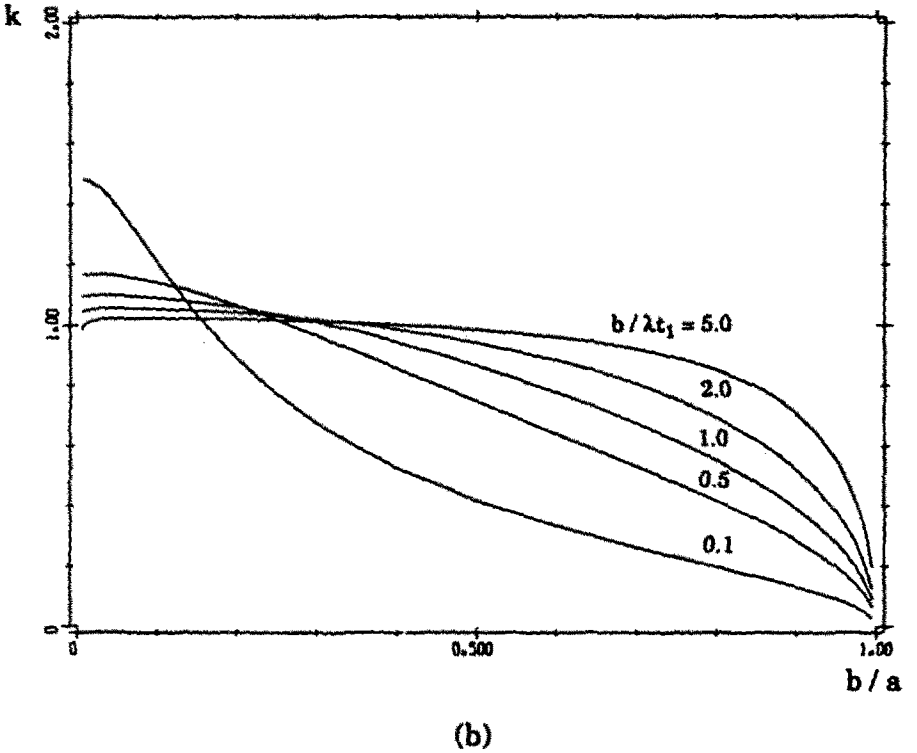

(b)

Fig. 8. Variation of the normalized stress intensity factor with respect to the crack geometric pattern. (a) Fixed a values. (b) Fixed b values.

On the other hand, for a fixed value of b, k is rather insensitive as new parallel cracks emerge (or as a decreases), as shown in Fig. 8(b). This implies that the intralaminar crack density can increase dramatically without a substantial rise in the applied load level. Consequently, after initial delamination, the damage in the composite is dominated by the increase of the intralaminar crack population, as frequently observed in experiments. The multiplication of intralaminar cracks proceeds as the load increases until the plateau region in Fig. 8(a) is reached. Then, a substantial amount of delamination becomes inevitable. This switch of cracking modes from intralaminar to interlaminar is usually termed as the *characteristic damage state*. From (49), (51) and the stress intensity factor criterion (52), the occurrence of the characteristic damage state can be predicted at a load level of:

$$\hat{\sigma}_{1,3} = \frac{1}{\sqrt{t_1}} K_{1c,3c}. \tag{53}$$

After the characteristic damage state, the remaining linking ligaments between neighbouring plies return to a stable situation, as shown in both Fig. 8(a,b).

One way to estimate the crack geometric parameters a_c and b_c at the characteristic damage state is the *equal descending speed of k* criterion postulated as:

$$\frac{\partial}{\partial a} k\left(\frac{a_c}{\lambda t_1}, \frac{b_c}{\lambda t_1}\right) = \frac{\partial}{\partial b} k\left(\frac{a_c}{\lambda t_1}, \frac{b_c}{\lambda t_1}\right). \tag{54}$$

A more comprehensive approach relies on the energy released during the development of damage. The interfacial displacement

$$u(x_1) = \frac{\lambda \tilde{\varepsilon} t_1}{\pi} \int_{-1}^{1} \ln \left| \frac{\sin[\eta(s-u)]}{\sin(\eta s)} \right| \tau(s)\, ds, \tag{55}$$

which occurs at the decohesion parts of the interlaminar boundary causes an elastic shrink-back at the intralaminar crack tip:

$$\delta_c = 2b[\tilde{\varepsilon} + u(a) - u(a-b)] = 2a\tilde{\varepsilon} h\left(\frac{a}{\lambda t_1}, \frac{b}{\lambda t_1}\right), \tag{56}$$

where

$$h\left(\frac{a}{\lambda t_1}, \frac{b}{\lambda t_1}\right) = \frac{b}{a} + \frac{\lambda t_1}{2ma} \sum_{k=1}^{m} \ln \frac{\sin[\eta(1+s_k)]}{\sin[\eta(1-s_k)]} B(s_k). \tag{57}$$

The values for h are given in Table 6. The macroscopic damage strains produced by the delamination are:

Table 6. Normalized damage strain h in the interaction case

$2b/\lambda t_1$	$2a/\lambda t_1 = 10.00$	12.00	15.00	20.00	30.00
0.125	0.11678	0.09703	0.07726	0.05750	0.03781
0.250	0.14919	0.12464	0.09907	0.07395	0.04885
0.500	0.19748	0.16464	0.13162	0.09847	0.06527
1.000	0.27359	0.22860	0.18315	0.13734	0.09130
2.000	0.39979	0.33528	0.26949	0.20268	0.13515
3.000	0.51185	0.43085	0.34735	0.26189	0.17501
5.000	0.71350	0.60596	0.49178	0.37262	0.24994
7.500	0.92702	0.80351	0.65976	0.50352	0.33930
9.000	1.01357	0.90850	0.75490	0.57938	0.39160
9.500	1.02183	0.93990	0.78556	0.60427	1.40887
9.750	0.01659	0.95461	0.80067	0.61664	0.41747
9.875	0.01012	0.96167	0.80816	0.62286	0.42177

$$\bar{\varepsilon}^{D}_{11,13} = \bar{\varepsilon} h\left(\frac{a}{\lambda t_1}, \frac{b}{\lambda t_1}\right). \tag{58}$$

Similar expressions can be obtained for the other family of plies. Then by employing (4), (5) and (6), we have:

$$\bar{M}^{-1}_{11,33} = c_{2,1}E_z + c_{1,2}\frac{E\left[1-h\left(\frac{a}{\lambda t_1}, \frac{b}{\lambda t_1}\right)\right]}{1-E\hat{v}^2\bar{\varepsilon}^{(1)}h\left(\frac{a}{\lambda t_1}, \frac{b}{\lambda t_1}\right)},$$

$$\bar{M}^{-1}_{55} = G_z\left[1-h\left(\frac{a}{\lambda t_1}, \frac{b}{\lambda t_1}\right)\right]. \tag{59}$$

The energy released per unit volume by forming joint intralaminar and interlaminar damage can be estimated through a holding stress approach:

$$U_{1,3} = \tfrac{1}{2}\bar{\varepsilon} h\left(\frac{a}{\lambda t_1}, \frac{b}{\lambda t_1}\right)(\bar{\sigma}, \bar{\tau}), \tag{60}$$

which can be transformed to the crack surface energy and the interfacial energy in the spirit of the Griffith criterion:

$$\frac{t_1\gamma_c + 4b\gamma_i}{ah\left(\frac{a}{\lambda t_1}, \frac{b}{\lambda t_1}\right)} = \frac{\bar{\sigma}\bar{\varepsilon}}{2}, \tag{61}$$

and a similar expression for the anti-phase shear case; γ_c and γ_i are the specific surface and interfacial energy, respectively. Aside from the material parameters, the right-hand side of (61) depends on the loading, whereas the left-hand side of (61) relies on the crack geometry. The energy conservation equation (61), in combination with the delamination condition:

$$\hat{\sigma}_1\sqrt{t_1}k\left(\frac{a}{\lambda t_1}, \frac{b}{\lambda t_1}\right) = K_{1c}, \tag{62}$$

may provide the laws governing the evolution of the crack geometry.

6. ATTENUATION OF INTERLAMINAR SHEAR SINGULARITY

The physical significance of the perturbed equation (37) lies on the attenuation of the interlaminar shear stress singularity near the bonding edges. As a first order approximation, (37) is replaced by:

$$f_\varepsilon(u) - \varepsilon^2 f_\varepsilon''(u) = f(u), \quad f_\varepsilon(\pm 1) = 0, \tag{63}$$

where $f(u)$ is the solution of (42). It was shown by Vekua (1961) that such a direct iteration results in a uniformly valid asymptotic solution for the singular integrodifferential equation (37). The solution of (63) is straightforward:

$$f_\varepsilon(u) = \frac{1}{2\varepsilon}\left[\int_{-1}^{u} e^{(s-u)/\varepsilon} f(s)\,ds + \int_{u}^{1} e^{(u-s)/\varepsilon} f(s)\,ds - \frac{\cosh(u/\varepsilon)}{\cosh(1/\varepsilon)}\int_{-1}^{1} e^{(s-1)/\varepsilon} f(s)\,ds\right]. \quad (64)$$

The interlaminar shear stress can be obtained by differentiation:

$$\tau_\varepsilon(u) \approx \frac{1}{\varepsilon}\left[\cosh\left(\frac{1-u}{\varepsilon}\right)\int_{-1}^{1} e^{-(1-s)/\varepsilon}\tau(s)\,ds + \int_{u}^{1} \sinh\left(\frac{u-s}{\varepsilon}\right)\tau(s)\,ds\right], \quad (65)$$

for small ε. An important consequence by incorporating the shear deformation mode into the thin ply is the removal of the interlaminar shear stress singularity at the bonding edges. A bounded edge shear stress can be calculated through:

$$\tau_\varepsilon(1) = \frac{1}{\varepsilon}\int_{-1}^{1} e^{-(1-s)/\varepsilon}\tau(s)\,ds. \quad (66)$$

At the other extreme, one can prove that:

$$\tau_\varepsilon(u) \to \tau(u), \quad (67)$$

for sufficiently large $r = (1-u)\varepsilon$; this grants $\tau(u)$ the status of the outer solution of τ_ε. Equation (66) clearly demonstrates that the bonding edge stress is influenced by the outer solution $\tau(u)$ through a fast decaying weight function, like a non-local relation. A very rough estimate, in order to obtain the inner approximation of τ_ε, is to assume a one term expansion for τ:

$$\tau(u) \approx \sqrt{\frac{2}{\pi\Lambda}}\frac{k}{\sqrt{1-u^2}}. \quad (68)$$

A convergent infinite series

$$\tau_\varepsilon \approx \frac{k}{\sqrt{\varepsilon\Lambda}}\sum_{i=0}^{\infty}\left[\frac{r^{2i}}{(2i)!} - \sqrt{\frac{2}{\pi}}\frac{(2r)^{2i+(3/2)}}{(4i+3)!!}\right], \quad (69)$$

is then obtained for small r; $t_\varepsilon(u)$ and its inner and outer expansion are shown in Fig. 9 for the parameter setting $a/(\lambda t_1) = 10$, $b/(\lambda t_1) = 5$, $\varepsilon = 0.05$. It is observed that the perturbed solution $\tau_\varepsilon(u)$ and the outer solution $\tau(u)$ have to cross over in order to maintain the same static equilibrium. The highly localized nature of $\tau(u)$ (as demonstrated by our numerical solution) degrades the accuracy of the solution (69) based on the approximation (68). The importance of (69), however, lies in an explicit depiction of the parameter dependence of the real bonding edge stress:

$$\tau_{edge} = \beta k\bar{\varepsilon}\begin{cases}\sqrt{\dfrac{E\bar{E}}{2\bar{S}}}\left[\dfrac{3(1-\nu\nu_z)}{2(1+\nu)(1+\hat{\nu}^2)}\right]^{1/4} & \text{plane strain}\\ \sqrt{G_z}\left[\dfrac{3}{\bar{M}_{44}\bar{M}_{55}}\right]^{1/4} & \text{anti-plane shear}\end{cases} \quad (70)$$

where β is a factor slightly less than 1. Apparently, τ_{edge} depends on the cracked laminate geometry only through the factor βk (which is usually about unity). Accordingly, a delamination criterion based on the shear stress singularity $K_{I,3}$ as (52) is equivalent to a more physically appealing delamination criterion based on the shear stress at the bonding edge.

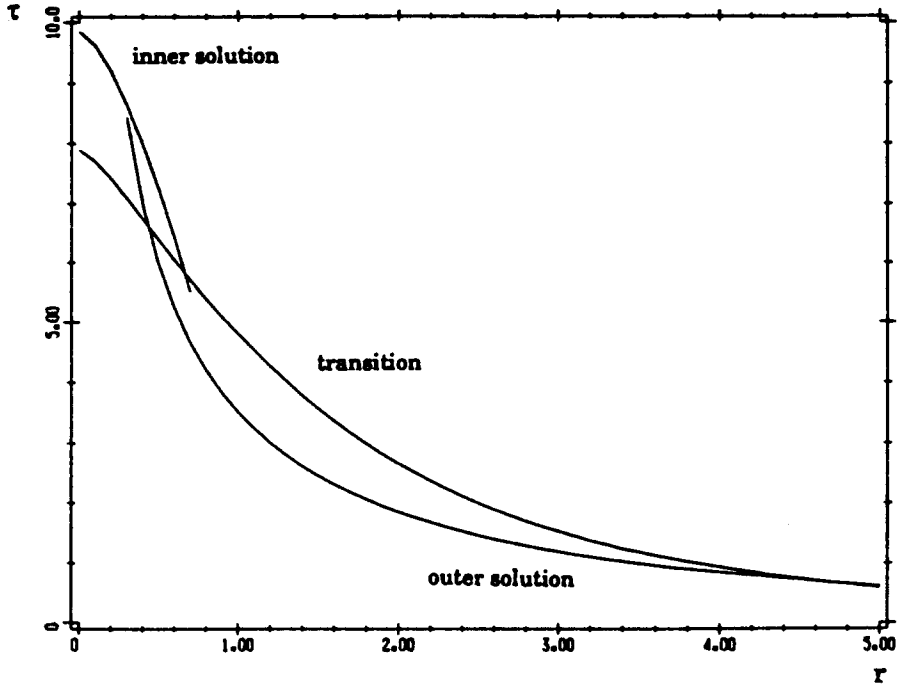

Fig. 9. Transition of the interlaminar shear stress from the inner solution to the outer solution.

7. IMPERFECT ADHESION MODEL

The damage modelling discussed in the previous sections tacitly leads to a pseudo-elastic damage behaviour. The damage is completely described by the change in the secant moduli, without any accommodation for the permanent damage strain and the formation of hysteresis loops, see the dashed lines in Fig. 10. These predictions, which are albeit

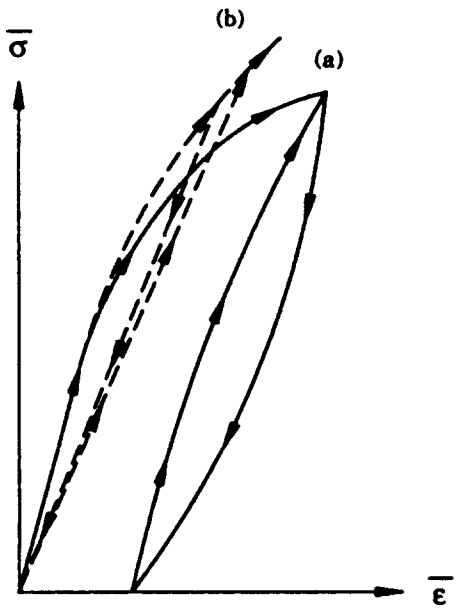

Fig. 10. Schematic macroscopic stress–strain curves for composite laminates predicted from theories with (a) and without (b) interlaminar slip.

inevitable from most nowaday composite damage theories, contradict the experimental findings for composite laminates. A physically sound remedy is to introduce a suitable localized slip deformation along the interlaminar boundary. It is conceivable to assume that the adhesion layer between two neighbouring plies can only support a maximum shear stress τ_s. When either τ_1 or τ_3 reaches τ_s, slip occurs without decohesion. For simplicity, here we assume that τ_s is insensitive to the slip deformation history, and we eliminate any coupling between τ_1 and τ_3 through a *yield condition* of the adhesion layer. The relaxations of the above-mentioned hypotheses would encourage more elaborate macroscopic constitutive models capable of describing phenomena such as gradually stabilized hysteresis loops and non-normality damage evolution. With the present simple model of imperfect adhesion, slip occurs at a distance r_s from both bonding edges when the absolute value of the shear stress reaches τ_s. Denoting this relative slip by:

$$\varepsilon_{slip} = \tilde{\varepsilon} e_{slip}, \tag{71}$$

then we can modify (42) as:

$$\frac{\Lambda}{\pi}\int_{-1}^{1} \eta \cot[\eta(s-u)]\tau(s)\,ds - \int_{-1}^{u} \tau(s)\,ds = 1 - e_{slip}(u), \quad u \in (-1, 1), \tag{72}$$

which is suitable for an arbitrary loading history. For monotonic loading, (72) can be clarified as:

$$\frac{\Lambda}{\pi}\int_{R-1}^{1-R} \eta \cot[\eta(s-u)]\tau(s)\,ds - \int_{R-1}^{u} \tau(s)\,ds = 1 - \omega\left\{R + \frac{\Lambda}{\pi}\ln\frac{\sin[\eta(1+u)]\sin[\eta(1-u)]}{\sin[\eta(1-R+u)]\sin[\eta(1-R-u)]}\right\}, \tag{73}$$

in the current non-slipping region $(R-1, 1-R)$, where:

$$R = \frac{r_s}{a-b}, \quad \omega = \frac{\tau_s}{\tilde{\tau}},$$

$$\tilde{\tau} = \Lambda\tilde{\varepsilon}\frac{\tilde{E}}{2\tilde{S}} \quad \text{plane strain},$$

$$\tilde{\tau} = \Lambda\tilde{\varepsilon}(\tilde{M}_{44}\tilde{M}_{55})^{-1/2} \quad \text{anti-plane shear}. \tag{74}$$

Equation (73) serves as the governing equation to solve $\tau(s)$. The result can be substituted back to evaluate e_{slip}:

$$e_{slip}(u) = 1 - \omega\left\{1 - u + \frac{\Lambda}{\pi}\ln\frac{\sin[\eta(1+u)]\sin[\eta(1-u)]}{\sin[\eta(u+1-R)]\sin[\eta(u-1-R)]}\right\} - \frac{\Lambda}{\pi}\int_{R-1}^{1-R} \eta \cot[\eta(s-u)]\tau(s)\,ds, \quad u \in (1-R, 1). \tag{75}$$

The relative slip between interlaminar crack tips is given by:

$$\delta_p = 2\tilde{\varepsilon}(a-b)\Delta_p, \tag{76}$$

where

$$\Delta_p = \int_{1-R}^{1} e_{slip}(u)\,du. \tag{77}$$

Equations (72) and (77) can be converted to the standard integrals:

$$\frac{\Lambda}{\pi}\int_{-1}^{1} \hat{\eta}\cot[\hat{\eta}(s-u)]\tau(\hat{s})\,d\hat{s} - (1-R)\int_{-1}^{\hat{u}} \tau(\hat{s})\,d\hat{s}$$
$$= 1-\omega\left\{R+\frac{\Lambda}{\pi}\ln\frac{\sin[\hat{\eta}(\alpha+\hat{u})]\sin[\eta(\alpha-\hat{u})]}{\sin[\hat{\eta}(1+\hat{u})]\sin[\hat{\eta}(1-\hat{u})]}\right\}, \quad \hat{u}\in(-1,1), \tag{78}$$

$$\Delta_p = R-\omega\left\{\frac{R^2}{2}+\frac{\Lambda}{\pi}\int_0^R \ln\frac{\sin[\eta(2-v)]}{\sin[\eta(2-R-v)]}\,dv\right\} - \frac{\Lambda}{\pi}(1-R)\int_{-1}^{1}\ln\frac{\sin[\hat{\eta}(\alpha-\hat{s})]}{\sin[\hat{\eta}(1-\hat{s})]}\tau(\hat{s})\,d\hat{s}, \tag{79}$$

by the variables' transformations:

$$u=(1-R)\hat{u}, \quad s=(1-R)\hat{s}, \quad \tau(s)\to\tau(\hat{s}), \quad \eta=\frac{\hat{\eta}}{1-R}, \quad \alpha=\frac{1}{1-R}, \tag{80}$$

in order to facilitate the numerical calculation. A numerical scheme has been developed to solve $\tau(\hat{s})$ and R in (78). We first decompose $\tau(\hat{s})$ as:

$$\tau(\hat{s}) = \omega\left[\hat{s}-\frac{\sqrt{1-\hat{s}^2}}{1-R}G(\hat{s})\right], \tag{81}$$

where $G(\hat{s})$ is a skew-symmetric, bounded function. Its values on a set of discrete point $\hat{s}_k$ can be computed effectively by the following numerical scheme (Erdogan, 1980):

$$\frac{1}{2m+1}\sum_{k=1}^{m}(1-\hat{s}_k^2)\left\{\frac{2\Lambda\eta\sin(2\hat{\eta}\hat{s}_k)}{\cos(2\hat{\eta}\hat{s}_k)-\cos(2\hat{\eta}\hat{u}_j)} - \pi H(j-k-\tfrac{1}{2})\right\}G(\hat{s}_k) = g(\hat{u}_j), \quad j=1,\ldots,m,m+1, \tag{82}$$

where $\hat{s}_k$ and $\hat{u}_j$ are zeros of the Chebyshev polynomials $U_{2m}(\hat{s}_k)$ and $T_{2m+1}(\hat{u}_j)$:

$$\hat{s}_k = \cos\frac{k\pi}{2m+1}, \quad \hat{u}_j = \cos\left(\frac{j-\frac{1}{2}}{2m+1}\pi\right), \tag{83}$$

and the right-hand side function g is given by:

$$g(\hat{u}) = \omega^{-1}-R-\frac{1-R}{2}(1-\hat{u}^2) - \frac{\Lambda}{\pi}\left\{\ln\sin[\hat{\eta}(\alpha+\hat{u})]\sin[\hat{\eta}(\alpha-\hat{u})] - \int_{-1}^{1}\ln\sin[\hat{\eta}(\hat{s}-\hat{u})]\,d\hat{s}\right\}, \tag{84}$$

which is bounded uniformly for $\hat{u}\in(-1,1)$. For an assumed value of R, the first m equations in (82) become linear algebraic equations of $G(\hat{s}_k)$, $k=1,\ldots,m$, and can be solved immediately. The last equation ($j=m+1$) can be used for the iteration of R. The results for R are

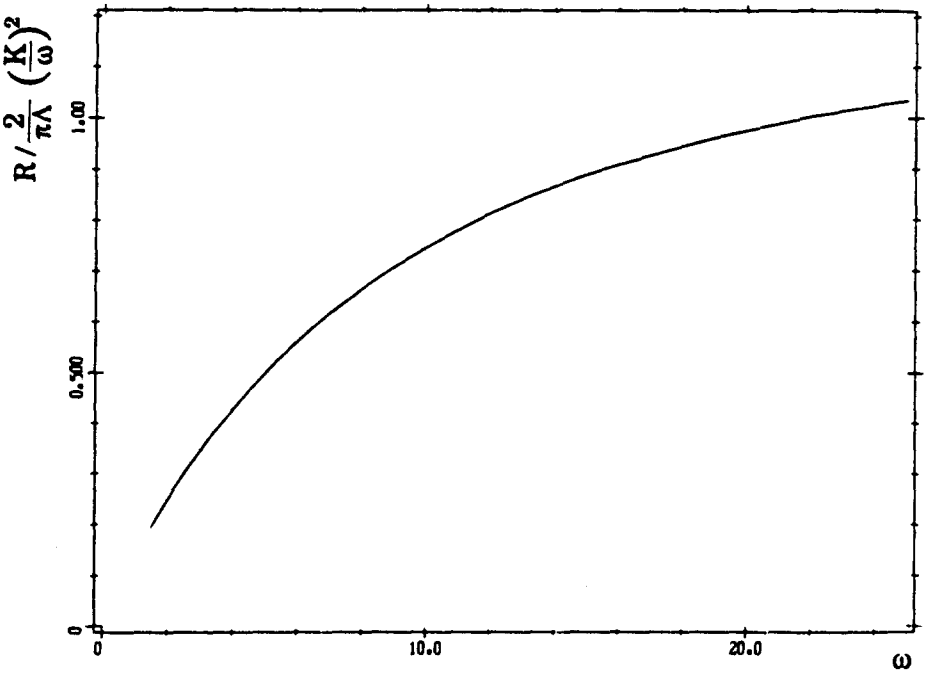

Fig. 11. Normalized slip length versus aspect ratio of slip stress ω. Case $a/(\lambda t_1) = 10$, $b/(\lambda t_1) = 5$.

normalized and plotted versus ω in Fig. 11 for $a/(\lambda t_1) = 10$ and $b/(\lambda t_1) = 5$. After obtaining $\tau(\hat{s})$ at discrete points $\hat{s}_k$, Δ_p can be evaluated through the formula (79) and is plotted against ω in Fig. 12. Both R and Δ_p decay rapidly with respect to ω.

In the case of small scale slipping (i.e. either large ω or small R), $\tau(\hat{s})$ in (72) may be approximated by:

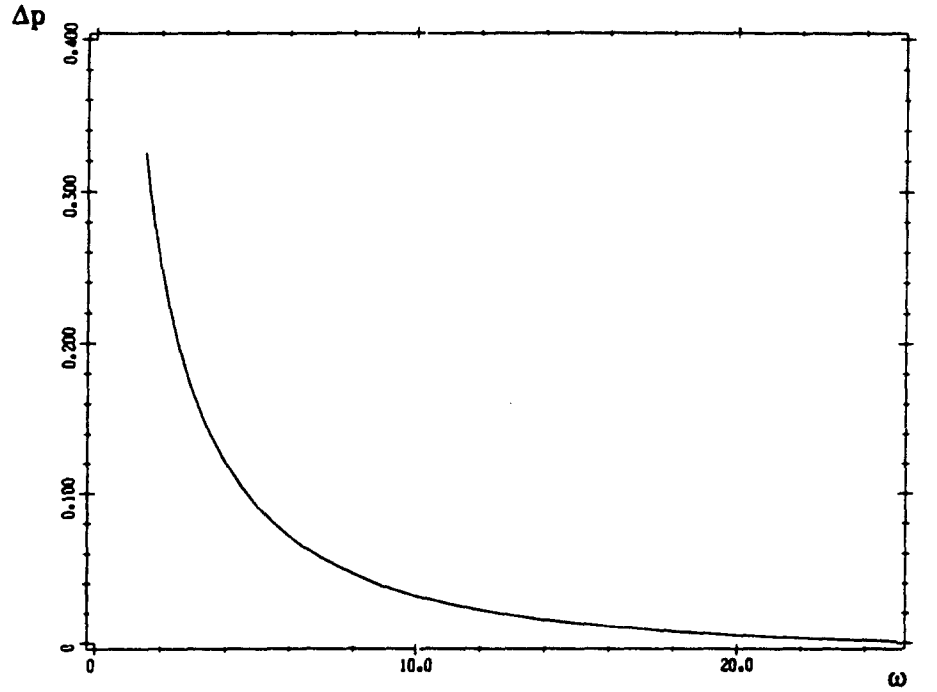

Fig. 12. Normalized intralaminar crack tip slip versus ω. Case $a/(\lambda t_1) = 10$, $b/(\lambda t_1) = 5$.

$$\tau(\hat{s}) \approx \tau_0[(1-r_f)\hat{s};\ \Lambda, \tilde{\eta}], \tag{85}$$

where $\tau_0(s;\ \Lambda, \tilde{\eta})$ is the perfect adhesion solution parameterized by Λ and $\tilde{\eta}$:

$$\frac{\Lambda}{\pi}\int_{-1}^{1} \tilde{\eta}\cot[\tilde{\eta}(s-u)]\tau_0(s)\,ds - \int_{-1}^{u} \tau_0(s)\,ds = 1, \quad u\in(-1, 1), \tag{86}$$

which is known from the previous calculation in Section 4. The approximation (85) is similar to the *small scale yielding* solution in fracture mechanics in the sense of Irwin; r_f is termed *fitting distance*, with the following definition:

$$\tau_0(1-r_f) = \frac{B(1-r_f)}{\sqrt{r_f(2-r_f)}} = \omega, \tag{87}$$

and the transformation parameter $\tilde{\eta}$ stands for $\hat{\eta}/(1-r_f)$. By global equilibrium (similar to the static equilibrium requirement in the case of small scale yielding in fracture mechanics), we determine R by insisting that (78) is satisfied at $u = 0$ (which is also consistent with our previous numerical scheme of R iterations):

$$\frac{\Lambda}{\pi}\int_{-1}^{1} \hat{\eta}\cot(\hat{\eta}\hat{s})\tau(\hat{s})\,d\hat{s} - (1-R)\int_{-1}^{0} \tau(\hat{s})\,d\hat{s} = 1-\omega\left[R + \frac{2\Lambda}{\pi}\ln\frac{\sin\eta}{\sin\hat{\eta}}\right]. \tag{88}$$

For small R or r_f, this equation reduces to:

$$R \approx r_f\left[2 + \frac{\displaystyle\int_0^{1-r_f} \tau_0(s)\,ds}{\omega\left(1+\dfrac{2\Lambda}{\pi}\eta\cot\eta\right)}\right] \approx 2r_f + O(r_f^{3/2}), \tag{89}$$

under the assumption that (87) is replaced by:

$$r_f \approx \frac{1}{\pi\Lambda}\left(\frac{k}{\omega}\right)^2. \tag{90}$$

When plotting R, normalized by the small scale slipping value $(2/\pi\Lambda)(k/\omega)^2$ in Fig. 11 we observe that their ratio approaches unity for large ω. A simplified formula of Δ_p under the small scale slipping assumption is given below:

$$\Delta_p \approx R - \omega R^2\left(\frac{1}{2} + \frac{\Lambda\eta}{\pi}\cot 2\eta\right) - \frac{\Lambda}{\pi}\frac{1-R}{1-r_f}\int_{r_f-1}^{1-r_f} \ln\frac{\sin(\eta-s\tilde{\eta})}{\sin(\hat{\eta}-s\tilde{\eta})}\tau_0(s)\,ds, \tag{91}$$

in order to complete this section.

8. MONOTONIC AND CYCLIC STRESS–STRAIN CURVES

Figure 13 shows schematically the formation of the macroscopic damage strain. The permission for a slip at the bonding edge will enhance the macroscopic damage strain in the broken ply:

$$\bar{\varepsilon}^{D}_{11,13} = \frac{\delta_e + \delta_p}{2a}, \tag{92}$$

indicating further softening as shown by the solid line in Fig. 10 in comparison with the dashed line for the perfect adhesion model in the case of monotonic loading. The difference between the two models becomes more pronounced when considering a cyclic load path as shown in Fig. 14. The critical issue here is that δ_p cannot be fully recovered in the model allowing interlaminar slip, so that a permanent damage strain remains after complete unloading.

To illustrate this point, let us consider the interlaminar shear stress distribution for a cyclic loading path, as shown in Fig. 14. First the loading increases monotonically from zero to $\bar{\sigma}_1$, with the interlaminar shear stress distribution shown by the dashed line. The slipped region has a length $R(\omega_1)$ and a slipped distance

$$\delta_{p1} = 2\tilde{\varepsilon}_1(a-b)\Delta_p(\omega_1), \quad \omega_1 = \frac{\tau_s}{\tilde{\tau}_1}. \tag{93}$$

The unloading process toward $\bar{\sigma}_2$ can be regarded as the superposition of a reverse loading $\Delta\bar{\sigma}$ with a reverse slip occurring at $2\tau_s$. The reverse slip caused by this procedure is:

$$\Delta\delta_p = -2\Delta\tilde{\varepsilon}(a-b)\Delta_p(\Delta\omega), \quad \Delta\omega = \frac{2\tau_s}{\Delta\tilde{\tau}}. \tag{94}$$

The remaining slip at the loading level $\bar{\sigma}_2$ is then given by:

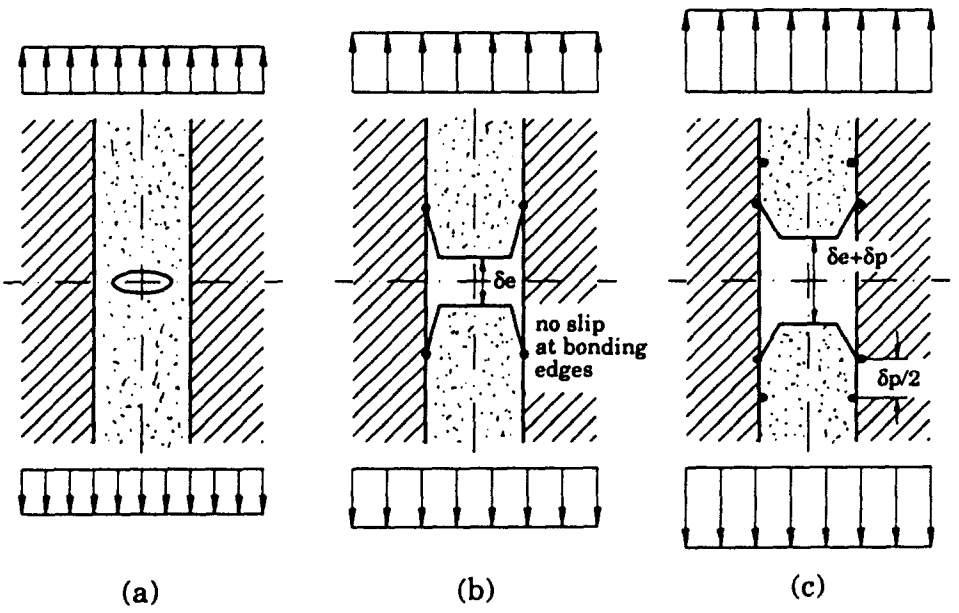

Fig. 13. Formation of macroscopic damage strain. (a) Initial intralaminar cracking. (b) Coupled intralaminar and interlaminar cracking, perfect adhesion. (c) Coupled intralaminar and interlaminar cracking, imperfect adhesion.

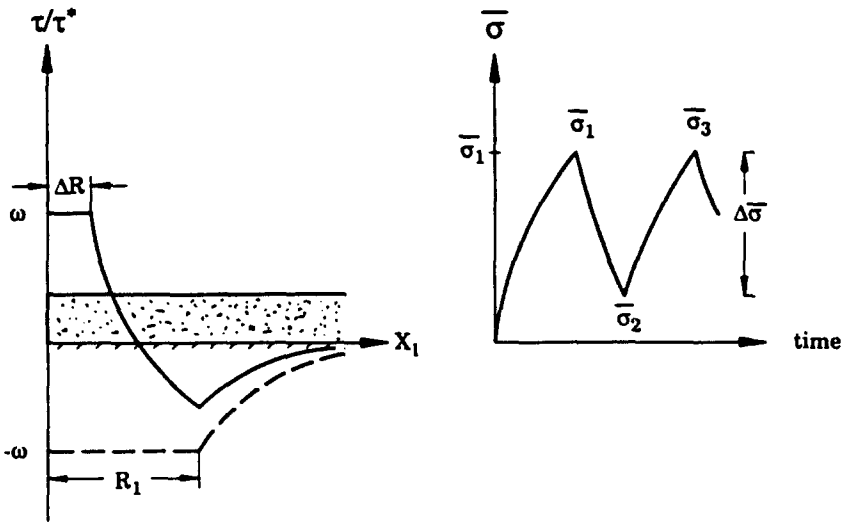

Fig. 14. Interlaminar shear stress distribution under cyclic loading.

$$\delta_{p2} = 2(a-b)\left[\bar{\varepsilon}_1 \Delta_p\left(\frac{\tau_s}{\bar{\tau}_1}\right) - \Delta\bar{\varepsilon}\Delta_p\left(\frac{2\tau_s}{\Delta\bar{\tau}}\right)\right]. \tag{95}$$

The residual slip caused by a maximum value for $\bar{\sigma}$ can be assessed by setting $\bar{\sigma}_2 = 0$:

$$\delta_p^r = 2(a-b)\bar{\varepsilon}\left[\Delta_p\left(\frac{\tau_s}{\bar{\tau}}\right) - \Delta_p\left(\frac{2\tau_s}{\bar{\tau}}\right)\right]. \tag{96}$$

From the rapidly decaying behaviour of Δ_p with respect to ω in Fig. 12, the majority of δ_p will remain after a complete unloading. Furthermore, as shown in the solid line of Fig. 14, there will be a residual interlaminar shear stress upon complete unloading.

The continued loading from $\bar{\sigma}_2$ to $\bar{\sigma}_3$ results in the re-occurrence of an interlaminar shear stress profile, as shown by the dashed line of Fig. 14. The subsequent cyclic loading will not distort the interlaminar shear stress alternation exhibited in Fig. 14. Consequently, the simple idealized slip model introduced here leads to an instantaneous stabilization of the hysteresis loop, as shown by the solid line in Fig. 10. The experimental data, however, sometimes indicate a gradual cyclic shifting of the loops, which might be explained by a more elaborate hardening rule for the slip stress τ_s.

9. CONCLUSIONS

(1) A micromechanics model anticipating the geometric features of damage in cross-ply composite laminates is developed; it furnishes the analytical predictions covering the damage evolution from the initial intralaminar cracking to the intralaminar–interlaminar interaction.

(2) The calculation for joint intralaminar–interlaminar cracks indicates an instantaneous initial delamination, a subsequent increase of intralaminar crack density, followed by a switch from the intralaminar cracking to substantial delamination as the load increases monotonically. The load level, as well as the geometries of the crack pattern corresponding to the characteristic damage state, can be determined.

(3) A square root singularity occurs at the bonding edges for the interlaminar shear stress, provided that the thin plies are analyzed under the plane stress assumption. This singularity can be eliminated by incorporating a shear deformation mode to the thin plies. The obtained finite value for the bonding edge stress is relatively insensitive to the ply

thickness and can be employed as a physically reasonable criterion governing the delamination process.

(4) By allowing a relative slip between the neighbouring plies, the macroscopic stress–strain curves of the composite laminate are obtained; they demonstrate features such as the coupled damage softening by cracking and localized slip, the formation of irreversible damage strain and stabilized hysteresis loops.

(5) Future investigations on a more sophisticated interfacial slip formulation, on localized fibre breaking caused by extra interfacial stress, as well as on the gradual rupture of favourably oriented plies, are needed for a complete understanding of the damage behaviour of composite laminates.

Acknowledgements—The authors would like to acknowledge the assistance of the French Ministry of Education for the creation and the sponsorship of this inter-university research program. The first author acknowledges the support by the Fok Yingtung Education Foundation for aiding his engagement in the research of material damage behaviour.

REFERENCES

Aboudi, J. (1987). Stiffness reduction of cracked solids. *Engng Fract. Mech.* **26**, 637–650.

Allen, D. H., Harris, C. E. and Groves, S. E. (1987). A thermomechanical constitutive theory for elastic composites with distributed damage—I. Theoretical development; —II. Application to matrix cracking in laminated composites. *Int. J. Solids Structures* **23**, 1310–1338.

Arutiunian, N. Kh. and Mkhitarian, S. M. (1969). Periodic contact problem for a half-plane with elastic laps (cover plates). *PMM* **33**, 813–843.

Bilby, B. A. and Eshelby, J. D. (1968). Dislocations and theory of fracture. In *Fracture* (Edited by H. Liebowitz), Vol. I, pp. 100–183. Academic Press, New York.

Budiansky, B., Hutchinson, J. W. and Evans, A. G. (1986). Matrix fracture in fiber-reinforced ceramics. *J. Mech. Phys. Solids* **34**, 167–189.

Delameter, W. R., Herrmann, G. and Barnett, D. M. (1975). Weakening of an elastic solid by a rectangular array of cracks. (Trans. ASME) *J. Appl. Mech.* **42**, 74–80.

Dvorak, G. J. and Laws, N. (1987). Analysis of progressive matrix cracking in composite laminates, II. First ply failure. *J. Comp. Mater.* **21**, 309–329.

Dvorak, G. J., Laws, N. and Hejazi, M. (1985). Analysis of progressive matrix cracking in composite laminates, I. Thermoelastic properties of a ply with cracks. *J. Comp. Mater.* **19**, 216–234.

Erdogan, F. (1980). Mixed boundary-value problems in mechanics. In *Mechanics Today* (Edited by S. Nemat-Nasser), Vol. 3, pp. 1–86. American Academy of Mechanics, Pergamon Press, New York.

Erdogan, F. and Civelek, M. B. (1974). Contact problems for an elastic reinforcement bonded to an elastic plate. (Trans. ASME) *J. Appl. Mech.* **41**, 1014–1018.

Groves, S. E., Harris, C. E., Highsmith, A. L., Allen, D. H. and Norvell, R. G. (1987). An experimental and analytical treatment of matrix cracking in crossply laminates. *Experimental Mechanics* **27**, 73–79.

Han, Y. M. and Hahn, H. T. (1988). A simplified analysis of transverse ply cracking in cross-ply laminates. *Comp. Mater. Tech.* **31**, 165–177.

Hashin, Z. (1985). Analysis of cracked laminates: a variational approach. *Mech. Mater.* **4**, 121–136.

Hashin, Z. (1986). Analysis of stiffness reduction of cracked cross ply laminate. *Engng Fract. Mech.* **25**, 771–778.

Hashin, Z. (1987). Analysis of orthogonally cracked laminates under tension. (Trans. ASME) *J. Appl. Mech.* **54**, 872–879.

Highsmith, A. L. and Reifsnider, K. L. (1982). Stiffness-reduction mechanisms in composite laminates. In *Damage in Composite Materials* (Edited by K. L. Reifsnider), pp. 103–117. ASTM, Philadelphia. STP 775.

Highsmith, A. L. and Reifsnider, K. L. (1986). Internal load distribution effects during fatigue loading of composite laminates. In *Composite Materials: Fatigue and Fracture* (Edited by H. T. Hahn), pp. 223–251. ASTM, Philadelphia. STP 907.

Jamison, R. D., Schulte, K., Reifsnider, K. L. and Stinchcomb, W. W. (1984). Characterization and analysis of damage mechanisms in tension–tension fatigue of graphite/epoxy laminates. In *Effects of Defects in Composite Materials* (Edited by D. J. Wilkins), pp. 21–55. ASTM, Philadelphia. STP 836.

Koiter, W. T. (1955). On the diffusion of load from a stiffener into a sheet. *Q. J. Mech. Appl. Math.* **8**, 164–178.

Laws, N. and Brockenbrough, J. R. (1987). The effect of micro-crack systems on the loss of stiffness of brittle solids. *Int. J. Solids Structures* **23**, 1247–1268.

Laws, N. and Dvorak, G. J. (1987). The effect of fibre breaks and aligned penny-shaped cracks on the stiffness and energy release rates in uni-directional composites. *Int. J. Solids Structures* **23**, 1269–1283.

Ogin, S. L., Smith, P. A. and Beaumont, P. W. R. (1985). Matrix cracking and stiffness reduction during the fatigue of a (0/90)$_s$ GFRP laminate. *Compos. Sci. Technol.* **22**, 23–31.

Talreja, R. (1985a). A continuum mechanics characterization of damage in composite materials. *Proc. Roy. Soc. London* **A399**, 195–216.

Talreja, R. (1985b). Transverse cracking and stiffness reduction in composite laminates. *J. Compos. Mater.* **19**, 355–375.

Vekua, I. N. (1945).On Prandtl's integro-differential equation. *PMM* **9**, 143–150.

Vekua, N. P. (1961). Linear integro-differential equations with small parameters for higher derivatives. In *Problems of Continuum Mechanics* (English Edition edited by J. R. M. Radok), pp. 592–601. SIAM, Philadelphia.

Yang, W. (1984). Shear stress concentration near the edge of a thin film deposited on substrate. Ph.D. Thesis, Brown University, Division of Engineering.